OPEN

IDEAL-IQ Magnetic Resonance Imaging Fat Fraction Quantification in Distinguishing Thymic Hyperplasia From Low-Risk Thymoma and Thymic Lymphoma in Adulthood: A Reliability and Efficacy Analysis

Jie Zhang, MD, Xiu-Long Feng, MD,* Yu-Hui Ma, MD,**
Jiang-Tao Lan, MD, Shu-Mei Wang, MD,† Guang Yang, MD, PhD,‡*
Yu-Chuan Hu, MD, and Guang-Bin Cui, MD, PhD**

Objectives: Detection of fat content in thymic lesions is essential to differentiate thymic hyperplasia from thymic tumors. This study assesses the reliability and efficacy of "iterative decomposition of water and fat with echo asymmetry and least-squares estimation quantization" IDEAL-IQ magnetic resonance sequence in distinguishing thymic hyperplasia from low-risk thymoma and thymic lymphoma in adulthood.

Methods: Thirty patients with thymic hyperplasia, 28 low-risk thymomas, and 13 thymic lymphomas were respectively enrolled. All subjects underwent conventional thorax magnetic resonance imaging and IDEAL-IQ sequence. The fat fraction (FF_{mean} and FF_{total}), signal intensity index, and R2* values of the lesions were compared for differences among 3 groups by the Mann-Whitney *U* and Kruskal-Wallis tests. Receiver operating characteristic curve analysis was performed to determine the differentiating efficacy.

Results: Both FF_{mean} and FF_{total} values in patients with thymic hyperplasia are significantly higher than those in patients with low-risk thymoma and thymic lymphoma (FF_{mean}: 26.41% vs 1.78% and 1.93%, FF_{total}: 27.67% vs 2.21% and 2.44%; both $P < 0.001$), whereas there was no significant difference in these values between low-risk thymomas and thymic lymphomas (both $P > 0.05$). Similarly, signal intensity index and R2* values of thymic hyperplasia were significantly higher than those of patients with low-risk thymoma and thymic lymphoma ($P < 0.001$). Receiver operating characteristic curve analysis showed that FF_{mean} had an area under the curve of 0.998, with a cutoff of 4.78% yielding 95.12% sensitivity and 100% specificity, and FF_{total} had an area under the curve of 0.994, with a cutoff of 8.57% yielding 97.56% sensitivity and 96.67% specificity in distinguishing thymic hyperplasia from tumors.

Conclusions: IDEAL-IQ sequence provides accurate fat quantitative parameters and can differentiate thymic hyperplasia from thymic neoplasms with robust efficacy and reliability.

Key Words: IDEAL-IQ, thymic hyperplasia, thymoma, thymic lymphoma

(*J Comput Assist Tomogr* 2025;49:431–439)

Thymic hyperplasia, thymic thymoma, and thymic lymphoma are the most common lesions of the anterior mediastinum.[1,2] The optimal treatment of the 3 is very different.[3] Except for a small number of patients accompanied by myasthenia gravis (MG) who do not respond to drug therapy and require surgical intervention, the vast majority of patients with thymic hyperplasia and MG can be cured using drugs.[4–6] Depending on the tumor's resectability, thymoma can be treated with surgery, chemotherapy, radiotherapy, or a combination of several treatment methods. Moreover, chemotherapy is the primary treatment for lymphoma. Consequently, it is essential to have an accurate diagnosis to formulate the optimal treatment strategy.

Some mass-like thymic hyperplasia often presents as a space-occupying lesion in the anterior mediastinum, lacking visible fat infiltration on conventional computed tomography (CT) or magnetic resonance (MR) images, overlapping with imaging findings of low-risk thymoma (type A, AB, and B1) or thymic lymphoma.[7,8] Normal and hyperplastic thymus contains microscopic fat, resulting in a signal drop on out-phase MR images, so chemical-shift imaging helps differentiate thymic hyperplasia from thymic neoplasms.[9–12] However, for some low-fat thymic hyperplasia, there is no signal intensity loss on the out-phase images.[13,14] Moreover, chemical-shift imaging is susceptible to T1/T2* and magnetic field inhomogeneities, resulting in inaccurate water-lipid separation. In addition, previous researchers acquired the mean chemical-shift ratio (CSR) normalized to the paraspinal muscle, which may have been affected by age and body mass index.[12] Meanwhile, the signal intensity index (SII), even though it does not require a reference

From the *Department of Radiology & Functional and Molecular Imaging Key Lab of Shaanxi Province; †Department of Pathology, and; and ‡Department of Thoracic Surgery, Tangdu Hospital, Air Force Medical University, Xi'an, Shaanxi, People's Republic of China.

Received for publication June 12, 2024; accepted September 12, 2024.

J.Z. and X.-L.F. have contributed equally to this work.

Correspondence to: Guang-Bin Cui, MD, PhD, Department of Radiology & Functional and Molecular Imaging Key Lab of Shaanxi Province, Tangdu Hospital, Air Force Medical University, Xi'an 710038, Shaanxi, People's Republic of China (e-mail: cgbtd@126.com; cuigbtd@fmmu.edu.cn). Yu-Chuan Hu, MD, Department of Radiology & Functional and Molecular Imaging Key Lab of Shaanxi Province, Tangdu Hospital, Air Force Medical University, Xi'an 710038, Shaanxi, People's Republic of China (e-mail: hyc3140@126.com).

This work was supported by the Science and Technology Innovation Development Foundation of Tangdu Hospital (no. 2021LCYJ013).

Our article did not receive funding for research from any of the following organizations: National Institutes of Health, Wellcome Trust, and Howard Hughes Medical Institute.

The authors declare no conflict of interest.

DOI: 10.1097/RCT.0000000000001688

TABLE 1. Clinical and Demographic Characteristics of the 71 Patients With Thymic Lesions

Patient Characteristics	TH (n = 30)	LRT (n = 28)	TL (n = 13)	*P*
Age, y				< 0.001*
Median (IQR)	28 (22–32)	53 (44–62)†	38 (27–49)	
Range	18–51	18–78	18–63	
Gender, n (%)				0.046‡
Male	5 (22.7)	10 (45.5)	7 (31.8)	
Female	25 (51.0)	18 (36.7)	6 (12.2)	
Initial major symptoms, n (%)				0.005‡
MG	15 (75.0)	5 (25.0)	0	
Respiratory symptoms	0	7 (70.0)	3 (30.0)	
Chest pain	3 (50.0)	1 (16.7)	2 (33.3)	
No symptoms	10 (35.7)	13 (46.4)	5 (17.9)	
Other	2 (28.6)	2 (28.6)	3 (42.9)	
Pathologic procedure, n (%)				< 0.001‡
Thoracotomy	0	6 (75.0)	2 (25.0)	
Thoracoscope	5 (17.9)	21 (75.0)	2 (7.1)	
Percutaneous biopsy	1 (9.1)	1 (9.1)	9 (81.8)	
Histological type, n (%)				
Thymoma				
Type A		2 (7.1)		
Type AB		19 (67.9)		
Type B1		7 (25.0)		
Thymic lymphoma				
T lymphoblastic lymphoma			3 (13.1)	
Diffuse large B-cell lymphoma			1 (7.7)	
Hodgkin lymphoma			3 (13.1)	
Non-Hodgkin lymphoma			2 (15.4)	
MALT lymphoma			4 (30.8)	

*$P < 0.05$ indicates a statistically significant difference among groups based on Kruskal-Wallis test.
†Represents significant differences among thymic hyperplasia, low-risk thymoma, and thymic lymphoma groups ($P < 0.05$).
‡$P < 0.05$ indicates a statistically significant difference among groups based on Fisher exact tests.
IQR indicates interquartile range; LRT, low-risk thymoma; MALT, mucosa-associated lymphoid tissue; TH, thymic hyperplasia; TL, thymic lymphoma.

tissue, still needs multiple measurement sites and calculations.[15] Therefore, it is necessary to validate new methods to quantify the fat components of thymic lesions accurately.

Recently, the clinical application of iterative decomposition of water and fat with echo asymmetry and least-squares estimation quantitation (IDEAL-IQ) sequence has made it possible to measure intratissue fat accurately and has been used to estimate fat fraction (FF).[16,17] IDEAL-IQ imaging enables the correction of effects caused by T2* and B0 field inhomogeneity, and all scans can be completed in a single breath hold.[18–20] This technique has been well documented in the liver,[18,21,22] pancreas,[23] bone marrow,[19,24–27] and salivary glands.[28] However, to our knowledge, no study has investigated the utility of the IDEAL-IQ sequence in quantifying the fat components of thymic lesions for differentiating thymic hyperplasia and thymic neoplasms.

Thus, the aims of this study are to retrospectively evaluate the usefulness of the IDEAL-IQ sequence in distinguishing thymic hyperplasia from low-risk thymoma and thymic lymphoma in adulthood, with a proposal of optimal threshold, and explore the added value of this sequence.

MATERIALS AND METHODS

Study Population

The local ethics committee approved this retrospective single-center study, and informed consent was waived. This study was conducted under the Declaration of Helsinki.

From November 2015 to July 2023, 71 patients with thymic hyperplasia, low-risk thymoma, and thymic lymphoma were included in this study. All patients included were older than 18 years. Conventional MR imaging (MRI) and IDEAL-IQ sequences of the thorax were performed in all patients. Demographic data were retrieved from electronic medical records.

Twenty-four patients with thymic hyperplasia have been confirmed by clinical follow-up and imaging findings, whereas others with thymic hyperplasia, low-risk thymoma (type A, AB, and B1), and thymic lymphoma have been confirmed by surgery or puncture pathology. The reference imaging diagnosis for rebound hyperplasia was as follows: thymus gland appeared at MRI as a soft-tissue diffuse enlargement of the thymus in a triangular or quadrilateral shape above the upper limit of normal for a given age.[15] The exclusion criteria for thymic hyperplasia and tumors were as follows: (*a*) based on CT or MRI, there is visible fat in the hyperplasia thymic tissue on conventional CT or MR image; (*b*) thymoma combined with thymic hyperplasia; (*c*) poor image quality or motion artifact; and (*d*) lesions smaller than 1.0 cm in diameter on axial plane, based on the longest diameter of the solid component or solid portion of complex mass. In addition, some patients with thymic tumor who received chemotherapy, radiotherapy, or other treatments before MRI were also excluded. Finally, 30 cases of thymic hyperplasia, 28 low-risk thymomas, and 13 thymic lymphomas were included in this study.

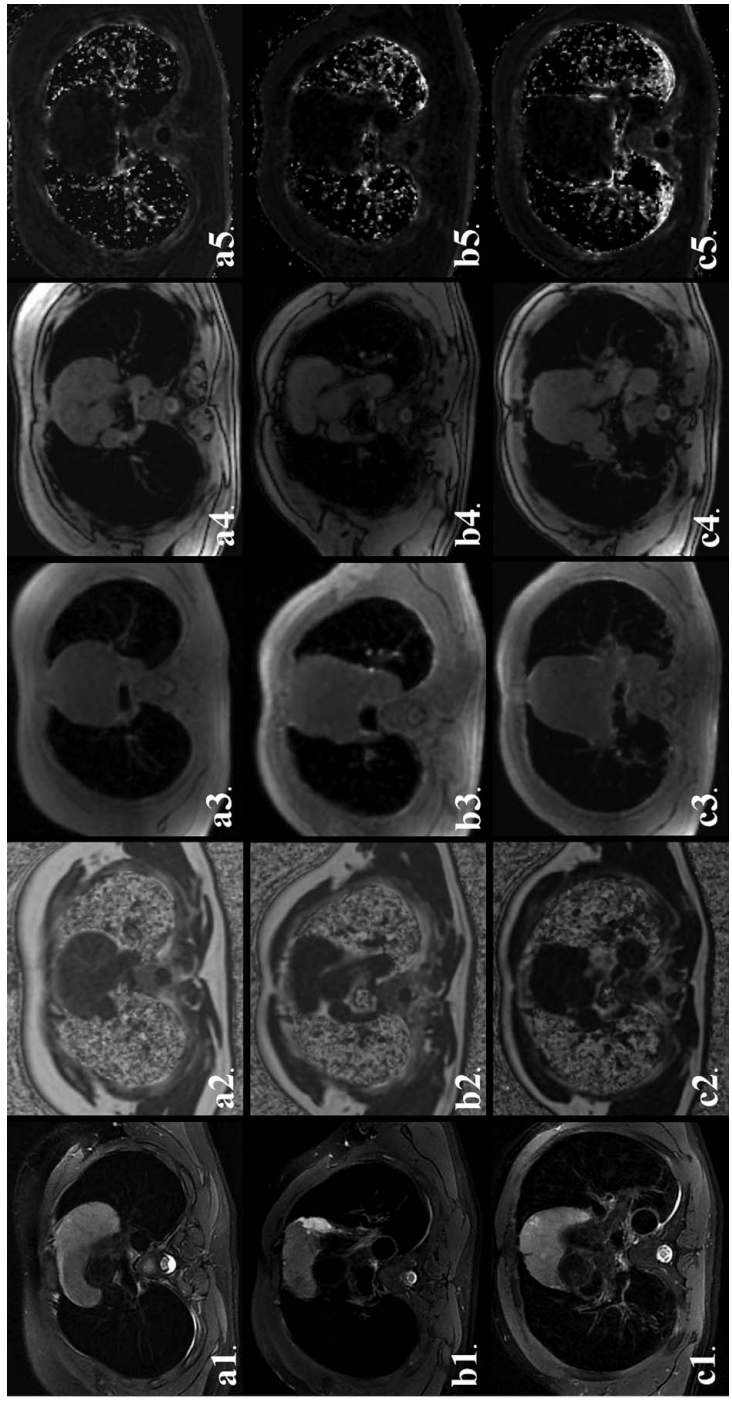

FIGURE 1. Representative MRI scans of patients with thymic hyperplasia, low-risk thymoma, and thymic lymphoma. A1–A5, A 19-year-old female patient with thymic hyperplasia. An anterior mediastinal mass grows from the midline to the sides on an axial fat-suppressed T2-weighted image (A1). Fat fraction (FF_{mean}) value was 11.88% (A2), SII value was 0.334 based on in-phase and out-phase images (A3, A4), and R2* value was 9.09 (A5). B1–B5, A 40-year-old man with type B1 thymoma (B1). FF_{mean} was 1.78% (B2), and SII was 0.004 based on in-phase and out-phase images (B3, B4), and R2* was 10.42 (B5). C1–C5, A 52-year-old man with thymic extranodal marginal zone lymphoma of mucosa-associated lymphoid tissue. An anterior mediastinal mass with an oval shape and smooth contours and expansion from midline to sides (C1). FF_{mean} was 0.37% (C2), and SII was 0.08 based on in-phase and out-phase images (C3, C4), and R2* was 29.17 (C5).

Thorax MRI Scan Protocol

All the MR examinations of the thorax were performed with the same scan protocol on a 3 T whole-body system (MR750; GE Healthcare, Milwaukee, WI) with a 40-mT/m maximum gradient capability and an 8-channel phased-array body coil. The subjects were examined in the supine position and entered head first. Respiratory bellows were applied to monitor breathing, and subjects were instructed to hold their breath during the image acquisition. A local shim box covering the whole thorax was applied to minimize the susceptibility artifacts. Conventional MRI and IDEAL-IQ sequences were performed in regular sequence during the same examination. The conventional MRI protocol included respiratory and electrocardiographic gating T1-weighted spin-echo imaging in the axial plane (T1-weighted imaging: repetition time [TR]/echo time [TE], 857/8 ms; matrix size, 288 × 160; field of view [FOV], 40 × 40 cm; the number of excitation [NEX], 1; slice thickness, 5 mm; gap, 0.5 mm), T2-weighted fast spin-echo imaging in the axial planes (TR/TE, 4000/81 ms; matrix size, 288 × 288; FOV, 40 × 40 cm; NEX, 1; slice thickness, 5 mm; gap, 0.5 mm) and coronal planes (TR/TE, 4200 s/78 ms; matrix size, 288 × 288; FOV, 40 × 40 cm; NEX, 2; slice thickness, 5 mm; gap, 1.0 mm), and axial T2-weighted turbo spin-echo imaging with fat suppression (TR/TE, 10,000/182 ms; matrix size, 320 × 320; FOV, 40 × 40 cm; NEX, 2; slice thickness, 5 mm; gap, 0.5 mm).

Subsequently, the IDEAL-IQ sequence can generate 6 groups of images, including water, fat, in-phase, out-phase, R2*, and FF map in 1 scan. The scan parameters were as follows: TR/TE, 5.9/6 ms; matrix size, 288 × 160; FOV, 42 × 42 cm; slice thickness, 5 mm; gap, 0.5 mm; NEX, 1.

Image Analysis

All MRI scans were analyzed on a GE ADW4.6 workstation (GE Healthcare). The parameters were measured independently by 2 radiologists (J.Z. and X.-L.F., with 7 and 12 years of chest MRI experience, respectively) blinded to the pathology or outcome of thymic lesions. The derived parameters of the IDEAL-IQ sequence include FF, SII, and R2*.

Two methods are used to draw the region of interest (ROI) for measuring FF value. First, on the level with the maximum display of thymic lesions in the FF image, 3 equally sized circular ROIs are drawn by hand (ROI range, 50–150 mm^2), and obvious cystic and necrotic areas should be avoided as much as possible. The system automatically obtains the FF value of the corresponding ROI, takes the average of 3 FF values, and records it as the FF_{mean}. Next, ROI is manually drawn on the 3 consecutive slices with the largest area of thymic lesions on the FF image, trying to cover the entire lesion as much as possible and paying attention to excluding adjacent tissues. The system automatically calculates the FF values of ROI for 3 levels and takes the average value to record as the FF_{total}.

On the in-phase and out-phase images, a circular ROI was manually drawn using an electronic cursor in the slice containing the largest cross-sectional area of thymic lesions, referring to the short time-inversion recovery sequence to avoid obvious cystic and necrotic areas. The system automatically calculates the signal intensity values of the ROI in the in-phase (SI_{in}) and out-phase images (SI_{out}). The SII value of the lesion is calculated according to Equation (1). Among them, tSI_{in} is the lesion signal intensity in the in-phase image, and tSI_{out} is the lesion signal intensity in the out-phase image.

$$SII = [(tSI_{in} - tSI_{out})/(tSI_{in})] \times 100\% \quad (1)$$

Similarly, an ROI was manually drawn on the R2* image, with the same size and position as on the in-phase and out-phase images, and the R2* value was automatically obtained.

Statistical Analyses

All statistical analyses were performed with IBM SPSS 26.0 software (IBM Corp, Armonk, NY). The Kolmogorov-Smirnov test was used to assess the normality. The Kruskal-Wallis test or χ^2 test was used to compare the differences in ages, gender, initial major symptoms, and pathologic procedures among groups. The FF, SII, and R2* values were compared for differences among defined groups with the Mann-Whitney U test. Receiver operating characteristic curves were performed to determine optimum thresholds for differentiating the defined groups based on various parameters and to calculate sensitivity, specificity, and area under the curve (AUC) values. Interobserver agreement between the 2 observers was analyzed using the interclass correlation coefficient (ICC) and the 95% Bland-Altman limits of agreement. ICCs were interpreted as follows: 0–0.20, poor agreement; 0.21–0.40, fair agreement; 0.41–0.60, moderate agreement; 0.61–0.80, good agreement; and 0.81–1.00, excellent agreement. $P < 0.05$ indicates a statistically significant difference.

RESULTS

Demographic Characteristics

Seventy-one patients were assigned to thymic hyperplasia (n = 30), low-risk thymoma (n = 28), and thymic lymphoma (n = 13). The demographic characteristics of the patients are summarized in Table 1. The final patients consisted of 22 men and 49 women. The median age of low-risk thymoma patients (53 years) was significantly higher than that of 28 years of thymic hyperplasia and 38 years of thymic lymphoma patients ($P < 0.001$). MG was found in patients with thymic hyperplasia (75%, 15/20) and low-risk thymoma (25.0%, 5/20), and no MG was found in thymic lymphoma patients. Respiratory symptoms were found in patients with low-risk thymoma (70.0%, 7/10) and thymic lymphoma (30.0%, 3/10) and were not seen in thymic hyperplasia patients. In addition, initial major symptoms include chest pain, no symptoms, and other symptoms found in different proportions in all patients.

As for the pathological procedure, only 6 cases (20.0%) of thymic hyperplasia were proven by surgery or biopsy pathology, while 24 cases (80.0%) were confirmed based on clinical and imaging. Other 41 tumor patients were all proven by the surgery or biopsy pathology. According to the World Health Organization pathological classification, 28 patients had low-risk thymomas (type A [n = 2], AB [n = 19], and B1 [n = 7]), and 13 thymic lymphomas, including T lymphoblastic lymphoma (n = 3), diffuse large B-cell lymphoma (n = 1), Hodgkin lymphoma (n = 3), non-Hodgkin lymphoma (n = 2), and mucosa-associated lymphoid tissue lymphoma (n = 4).

TABLE 2. Comparisons of FF, SII, and R2* Values Among Patients With Thymic Hyperplasia, Low-Risk Thymoma, and Thymic Lymphoma

Variables	TH	LRT	TL	*P*
FF_{mean} (%)	26.41 (15.66–37.66)*	1.78 (1.06–2.67)	1.93 (1.35–2.30)	<0.001†
FF_{total} (%)	27.67 (14.19–37.67)*	2.21 (1.37–3.11)	2.44 (1.85–4.57)	<0.001†
SII	0.47 (0.27–0.66)*	0.05 (0.04–0.09)	0.08 (0.06–0.11)	<0.001†
R2*	58.79 (40.94–74.43)*	22.35 (17.02–35.01)	25.62 (15.09–30.05)	<0.001†

The data are expressed as the median (P_{25}, P_{75}) deviation.
*Represents significant differences between thymic hyperplasia and thymoma or thymic lymphoma ($P < 0.05$).
†Comparisons among groups using Kruskal-Wallis test; $P < 0.05$ indicates a statistically significant difference among all groups.
LRT indicates low-risk thymoma; TH, thymic hyperplasia; TL, thymic lymphoma.

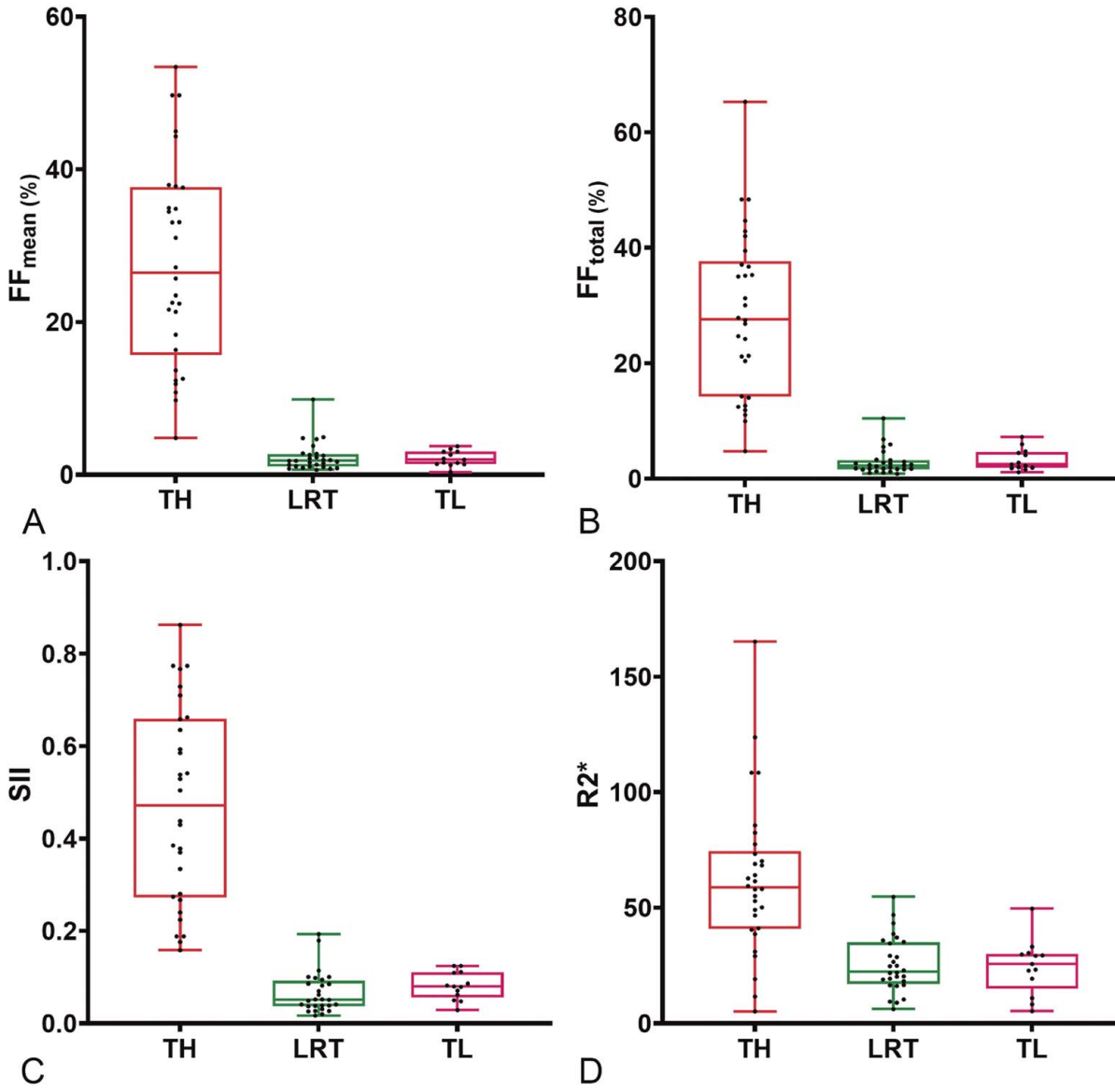

FIGURE 2. Box plots for values of FF_{mean} (A), FF_{total} (B), SII (C), and R2* (D) among thymic hyperplasia (TH), low-risk thymoma (LRT), and lymphoma (TL).

TABLE 3. Receiver Operating Characteristic Results of the IDEAL-IQ Parameters in Differentiating Thymic Hyperplasia and Low-Risk Thymoma or Thymic Lymphoma

Parameters	AUC	Sensitivity, %	Specificity, %	Cutoff Value	*P*
TH vs LRT					
FF_{mean} (%)	0.996	100.00	93.30	10.31	< 0.01
FF_{total} (%)	0.994	100.00	93.30	10.72	< 0.01
SII	0.993	92.86	100.00	0.14	< 0.01
R2*	0.877	89.29	80.00	39.58	< 0.01
TH vs TL					
FF_{mean} (%)	1.000	100.00	100.00	4.25	< 0.01
FF_{total} (%)	0.995	100.00	96.67	8.57	< 0.01
SII	1.000	100.00	100.00	0.14	< 0.01
R2*	0.882	92.31	83.33	35.84	< 0.01
TH vs LRT + TL					
FF_{mean} (%)	0.998	95.12	100.00	4.78	< 0.01
FF_{total} (%)	0.994	97.56	96.67	8.57	< 0.01
SII	0.995	95.12	100.00	0.14	< 0.01
R2*	0.879	87.80	83.33	37.85	< 0.01

LRT indicates low-risk thymoma; TH, thymic hyperplasia; TL, thymic lymphoma.

Comparison of FF, SII, and R* Value Among Thymic Hyperplasia, Low-Risk Thymomas, and Thymic Lymphomas

Representative MR parameter images (T2-weighted turbo spin-echo imaging with fat suppression, FF, in-phase, out-phase, and R2*) for patients with thymic hyperplasia, low-risk thymoma, and thymic lymphoma are shown in Figure 1. Comparisons of FF_{mean}, FF_{total}, SII, and R2* values among patients with thymic hyperplasia, low-risk thymoma, and thymic lymphoma are shown in Table 2 and Figure 2.

There were significant differences in FF_{mean}, FF_{total}, SII, and R2* values among groups with thymic hyperplasia, low-risk thymoma, and thymic lymphoma ($P < 0.001$). Both FF_{mean} and FF_{total} values in patients with thymic hyperplasia are significantly higher than those in patients with low-risk thymoma and thymic lymphoma (FF_{mean}: 26.41% vs 1.78% and 1.93%; FF_{total}: 27.67% vs 2.21% and 2.44%, both $P < 0.001$). The SII value of thymic hyperplasia was significantly higher than that that in patients with low-risk thymoma and thymic lymphoma (0.47 vs 0.05 and 0.08, $P < 0.001$). Similarly, The R2* value in patients with thymic hyperplasia was significantly higher than that in patients with low-risk thymoma and thymic lymphoma (58.79 vs 22.35 and 25.62, $P < 0.001$). By contrast, no significant statistical difference was shown between low-risk thymoma and thymic lymphoma ($P > 0.05$).

Diagnostic Efficacy Analysis

The results of the receiver operating characteristic analysis of the IDEAL-IQ parameters in differentiating thymic hyperplasia and low-risk thymoma or thymic lymphoma are shown in Table 3 and Figure 3. For FF_{mean}, FF_{total}, SII, and R2* values in differentiating thymic hyperplasia and thymic tumors (low-risk thymoma and thymic lymphoma), the values of AUC, sensitivity, specificity, and cutoff values are 0.998, 95.12%, 100%, and 4.78 for FF_{mean}; 0.994, 97.56%, 96.67%, and 8.57 for FF_{total}; 0.995, 95.12%, 100%, and 0.14 for SII; and 0.879, 87.50%, 83.33%, and 37.85 for R2*, respectively. In addition, all 4 parameters achieved higher efficacy for differentiating thymic hyperplasia and low-risk thymoma or thymic lymphoma.

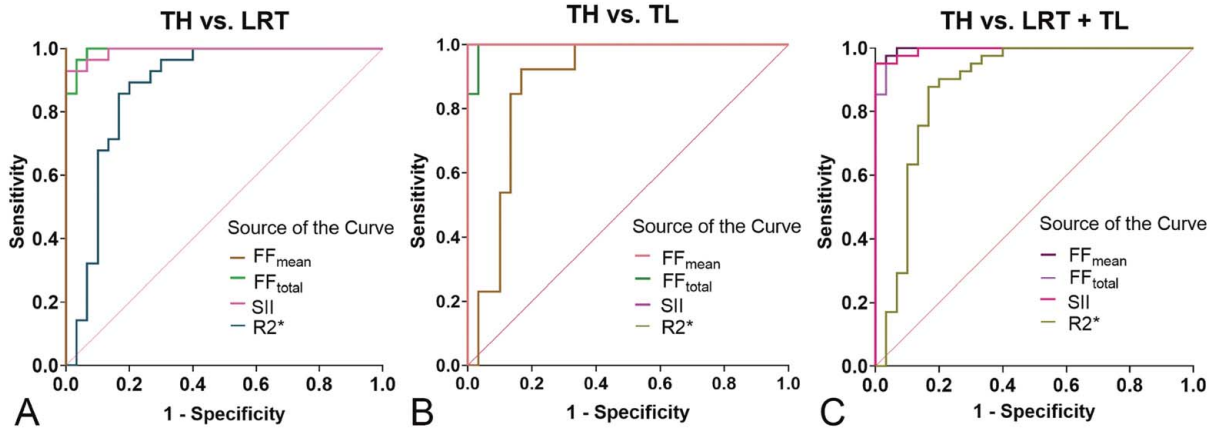

FIGURE 3. Receiver operating characteristic curves of FF, SII, and R2* values for differentiating the defined groups. A, Thymic hyperplasia (TH) versus low-risk thymoma (LRT), (B) TH versus thymic lymphoma (TL), and (C) TH versus LRT and TL.

TABLE 4. Reliability Analysis Between the 2 Observers' Measurements

Variable	ICC (n = 25)	95% CI	*P*
FF_{mean} (%)	0.993	0.989–0.996	< 0.001
FF_{total} (%)	0.990	0.985–0.994	< 0.001
SII	0.955	0.930–0.972	< 0.001
R2*	0.928	0.888–0.955	< 0.001

CI indicates confidence interval.

Interobserver Agreement for Quantitative Metrics

All quantitative parameters, including FF_{mean}, FF_{total}, SII, and R2* in thymic lesions, showed excellent interobserver agreement (all ICCs > 0.75). The ICC results are summarized in Table 4 and Figure 4.

DISCUSSION

This study evaluated whether the IDEAL-IQ sequence–derived parameter could differentiate thymic hyperplasia from low-risk thymoma and thymic lymphoma. The results revealed significantly higher FF and SII values in thymic hyperplasia than those in thymic tumors in the adult cohort, whereas there was no significant difference between low-risk thymoma and thymic lymphoma. In addition, we also determined the optimal cutoff value for each parameter, which could potentially be helpful in clinical practice regarding the differential diagnosis of thymic lesions before treatment.

In this study, thymic hyperplasia tends to occur in young women compared with thymoma and thymic lymphoma, consistent with previous research results.[29–31] Thymic hyperplasia and thymoma are often associated with numerous chronic inflammatory and autoimmune disorders.[29] The current study demonstrated that 75% of thymic hyperplasia and 25% of low-risk thymoma patients have MG, whereas there are no cases of MG in the lymphoma group.

Detecting microscopic fat within thymic lesions is essential in differentiating thymic hyperplasia from neoplasms.[15] The IDEAL-IQ sequence is a 3-dimensional sequence that enables water-fat separation, and it can accurately quantify proton density FF by correcting for the influence of T2* and B0 field inhomogeneity.[20,32] The current results indicate that the FF in thymic hyperplasia is higher than in low-risk thymoma and thymic lymphoma, which is associated with microscopic fat in thymus hyperplasia tissues.[33] Therefore, using FF can directly obtain the

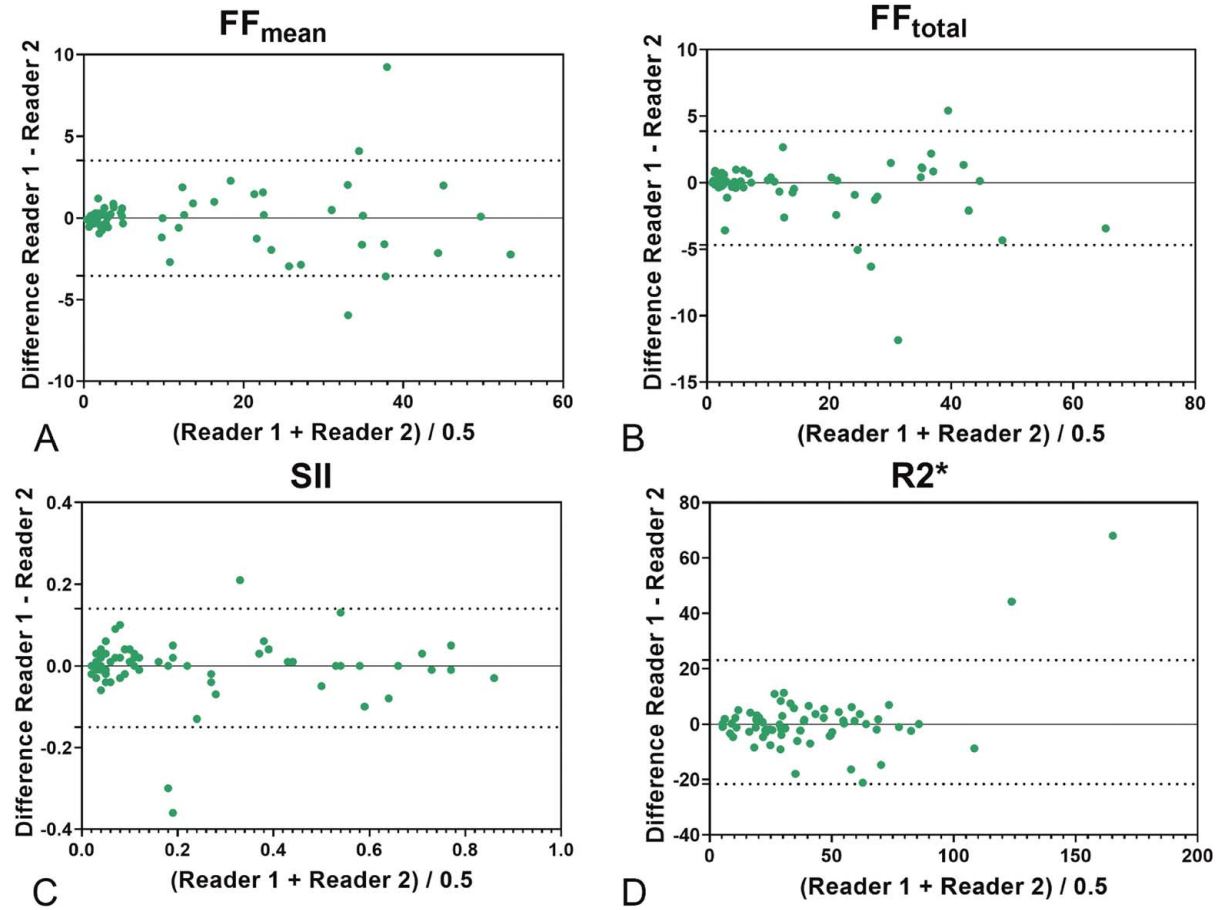

FIGURE 4. Bland-Altman analysis of 2 observers for FF, SII, and R2* values. Bland-Altman plots illustrate the interobserver variability for FF_{mean} (A), FF_{total} (B), SII (C), and R2* (D). The upper and lower reference lines indicate the upper and lower limits of agreement (95% confidence intervals).

fat content of the lesion, and the measurement is more accurate, simple, and fast. Hence, the IDEAL-IQ sequence seems to be the method for differentiating thymic hyperplasia from anterior mediastinal tumors.

Dual-echo chemical-shift MRI effectively proves the presence of an intravoxel mixture of fat and water in tissues by showing a loss of signal intensity on the out-phase image relative to the in-phase image.[12] Previous studies revealed that SII and CSR accurately distinguish thymic hyperplasia from tumors, although overlapped CSR values can occur in early adulthood.[15] The SII of thymic hyperplasia and thymic tumors accounted for 45.9% and 0.68%, respectively.[15] In addition to the FF value, we also evaluated the SII and obtained similar results as the above research, and the SIIs of thymic hyperplasia and low-risk thymoma and thymic lymphoma were 0.47, 0.05, and 0.08, respectively.

R2* can better reflect the iron content with tissue. Several studies[34–36] have shown that R2* positively correlates with tumor malignancy, and a hypoxic microenvironment is a hallmark in biology for solid tumors.[37] Interestingly, our study detected that the R2* content in the thymic hyperplasia was significantly higher than that in the thymic tumors. It seems to differ from the conclusions of relevant studies on tumors in other organs.[38–40] The possible reasons are that R2* estimation (R2* = 1/T2*) is inversely related to partial tissue pressure of oxygen[41] and reflects the paramagnetism of the tumor tissue, such as the presence of deoxygenated hemoglobin. Low-risk thymoma has a relatively low malignancy, slow tumor growth, and less obvious hypoxia, resulting in a lower R2* value.[42] This result may have some chance, and further studies are needed to elucidate the changes in R2* value in thymus lesions and its mechanism.

Furthermore, we assessed the diagnostic efficacy of FF and SII values in differentiating thymic hyperplasia, low-risk thymoma, and thymic lymphoma. The results showed that FF and SII values performed relatively well in distinguishing thymic hyperplasia from neoplasms, with an AUC of 0.998 and 0.995, respectively. One important consideration of using the IDEAL-IQ technique is obtaining repeatable patient data. In our study, all quantitative parameters, including FF_{mean}, FF_{total}, SII, and R2* in thymic lesions, showed excellent agreement between observers, indicating the reliability of the IDEAL-IQ parameters.

The present study has some limitations. First, the sample size was small; as a single-center and retrospective study, some diagnosed cases did not undergo IDEAL-IQ examination; further study with a larger sample of thymic lesion patients for elucidating this research question is warranted. Second, hand-drawn ROIs were used in the current study, and only the largest tumor layer was selected to delineate ROI and measure various quantitative parameters, which might have introduced a sampling bias; the application of image texture analysis based on whole lesion may be necessary in future research to verify the robustness of IDEAL-IQ results.

CONCLUSIONS

The IDEAL-IQ sequence provides accurate fat quantitative parameters, which could potentially be helpful in clinical practice regarding differentiating thymic hyperplasia from low-risk thymoma and thymic lymphoma before treatment.

REFERENCES

1. Punga AR, Maddison P, Heckmann JM, et al. Epidemiology, diagnostics, and biomarkers of autoimmune neuromuscular junction disorders. *Lancet Neurol*. 2022;21:176–188.
2. Marx A, Chan JK, Coindre JM, et al. The 2015 World Health Organization classification of tumors of the thymus: continuity and changes. *J Thorac Oncol*. 2015;10:1383–1395.
3. Fang W, Fu J, Shen Y, et al. Management of thymic tumors—consensus based on the Chinese Alliance for research in thymomas multi-institutional retrospective studies. *J Thorac Dis*. 2016;8:641–645.
4. Huang X, Liu WB, Men LN, et al. Clinical features of myasthenia gravis in southern China: a retrospective review of 2,154 cases over 22 years. *Neurol Sci*. 2013;34:911–917.
5. Bi Z, Zhan J, Zhang Q, et al. Clinical and immune-related factors associated with exacerbation in adults with well-controlled generalized myasthenia gravis. *Front Immunol*. 2023;14:1177249.
6. Uzawa A, Kanai T, Oda F, et al. Frequency and features of myasthenia gravis developing after thymectomy. *Eur J Neurol*. 2020;27:175–180.
7. Porubsky S, Popovic ZV, Badve S, et al. Thymic hyperplasia with lymphoepithelial sialadenitis (LESA)–like features: strong association with lymphomas and non-myasthenic autoimmune diseases. *Cancers (Basel)*. 2021;13:315.
8. Li HR, Gao J, Jin C, et al. Comparison between CT and MRI in the diagnostic accuracy of thymic masses. *J Cancer*. 2019;10:3208–3213.
9. McInnis MC, Flores EJ, Shepard J-AO, et al. Pitfalls in the imaging and interpretation of benign thymic lesions: how thymic MRI can help. *AJR Am J Roentgenol*. 2016;206:W1–W8.
10. Priola AM, Gned D, Veltri A, et al. Chemical shift and diffusion-weighted magnetic resonance imaging of the anterior mediastinum in oncology: current clinical applications in qualitative and quantitative assessment. *Crit Rev Oncol Hematol*. 2016;98:335–357.
11. Priola AM, Priola SM, Giraudo MT, et al. Chemical-shift and diffusion-weighted magnetic resonance imaging of thymus in myasthenia gravis: usefulness of quantitative assessment. *Invest Radiol*. 2015;50:228–238.
12. Inaoka T, Takahashi K, Mineta M, et al. Thymic hyperplasia and thymus gland tumors: differentiation with chemical shift MR imaging. *Radiology*. 2007;243:869–876.
13. Priola AM, Gned D, Marci V, et al. Diffusion-weighted MRI in a case of nonsuppressing rebound thymic hyperplasia on chemical-shift MRI. *Jpn J Radiol*. 2015;33:158–163.
14. Ackman JB, Mino-Kenudson M, Morse CR. Nonsuppressing normal thymus on chemical shift magnetic resonance imaging in a young woman. *J Thorac Imaging*. 2012;27:W196–W198.
15. Priola AM, Priola SM, Ciccone G, et al. Differentiation of rebound and lymphoid thymic hyperplasia from anterior mediastinal tumors with dual-echo chemical-shift MR imaging in adulthood: reliability of the chemical-shift ratio and signal intensity index. *Radiology*. 2015;274:238–249.
16. Reeder SB, Wen Z, Yu H, et al. Multicoil Dixon chemical species separation with an iterative least-squares estimation method. *Magn Reson Med*. 2004;51:35–45.
17. Liau J, Shiehmorteza M, Girard OM, et al. Evaluation of MRI fat fraction in the liver and spine pre and post SPIO infusion. *Magn Reson Imaging*. 2013;31:1012–1016.
18. Eskreis-Winkler S, Corrias G, Monti S, et al. IDEAL-IQ in an oncologic population: meeting the challenge of concomitant liver fat and liver iron. *Cancer Imaging*. 2018;18:51.
19. Aoki T, Yamaguchi S, Kinoshita S, et al. Quantification of bone marrow fat content using iterative decomposition of water and fat with echo asymmetry and least-squares estimation (IDEAL): reproducibility, site variation and correlation with age and menopause. *Br J Radiol*. 2016;89:20150538.

20. Tang A, Tan J, Sun M, et al. Nonalcoholic fatty liver disease: MR imaging of liver proton density fat fraction to assess hepatic steatosis. *Radiology*. 2013;267:422–431.
21. Corrias G, Krebs S, Eskreis-Winkler S, et al. MRI liver fat quantification in an oncologic population: the added value of complex chemical shift-encoded MRI. *Clin Imaging*. 2018;52: 193–199.
22. Chen R, Bai Y, Liu T, et al. Evaluation of glypican-3 expression in hepatocellular carcinoma by using IDEAL IQ magnetic resonance imaging. *Acad Radiol*. 2021;28:e227–e234.
23. Wen Y, Chen C, Kong X, et al. Pancreatic fat infiltration, β-cell function and insulin resistance: a study of the young patients with obesity. *Diabetes Res Clin Pract*. 2022;187:109860.
24. Huang Y, Wang L, Luo B, et al. Associations of lumber disc degeneration with paraspinal muscles myosteatosis in discogenic low back pain. *Front Endocrinol*. 2022;13:891088.
25. Ma Q, Cheng X, Hou X, et al. Bone marrow fat measured by a chemical shift-encoded sequence (IDEAL-IQ) in patients with and without metabolic syndrome. *J Magn Reson Imaging*. 2021; 54:146–153.
26. Jeon KJ, Lee C, Choi YJ, et al. Assessment of bone marrow fat fractions in the mandibular condyle head using the iterative decomposition of water and fat with echo asymmetry and least-squares estimation (IDEAL-IQ) method. *PloS One*. 2021;16: e0246596.
27. Watanabe D, Kimura T, Yanagida K, et al. Feasibility of assessing male osteoporosis using MRI IDEAL-IQ sequence of proximal femur in prostate cancer patients. *Aging Male*. 2022; 25:228–233.
28. Su GY, Wang CB, Hu H, et al. Effect of laterality, gender, age and body mass index on the fat fraction of salivary glands in healthy volunteers: assessed using iterative decomposition of water and fat with echo asymmetry and least-squares estimation method. *Dentomaxillofac Radiol*. 2019;48:20180263.
29. Priola AM, Priola SM. Imaging of thymus in myasthenia gravis: from thymic hyperplasia to thymic tumor. *Clin Radiol*. 2014;69:e230–e245.
30. Yang J, Liu C, Li T, et al. Prognosis of thymectomy in myasthenia gravis patients with thymus hyperplasia. *Int J Neurosci*. 2017;127:785–789.
31. Chang S, Hur J, Im DJ, et al. Volume-based quantification using dual-energy computed tomography in the differentiation of thymic epithelial tumours: an initial experience. *Eur Radiol*. 2017;27:1992–2001.
32. Li Y, Xiong Y, Hou B, et al. Detection of erosions and fat metaplasia of the sacroiliac joints in patients with suspected sacroiliitis using a chemical shift-encoded sequence (IDEAL-IQ). *Eur J Radiol*. 2023;158:110641.
33. Ackman JB, Wu CC. MRI of the thymus. *AJR Am J Roentgenol*. 2011;197:W15–W20.
34. Wang Y, Shen Y, Hu X, et al. Application of R2* and apparent diffusion coefficient in estimating tumor grade and T category of bladder cancer. *AJR Am J Roentgenol*. 2020; 214:383–389.
35. Liu M, Guo X, Wang S, et al. BOLD-MRI of breast invasive ductal carcinoma: correlation of R2* value and the expression of HIF-1α. *Eur Radiol*. 2013;23:3221–3227.
36. Shi GZ, Chen H, Zeng WK, et al. R2* value derived from multi-echo Dixon technique can aid discrimination between benign and malignant focal liver lesions. *World J Gastroenterol*. 2021;27:1182–1193.
37. Tatum JL, Kelloff GJ, Gillies RJ, et al. Hypoxia: importance in tumor biology, noninvasive measurement by imaging, and value of its measurement in the management of cancer therapy. *Int J Radiat Biol*. 2006;82:699–757.
38. Chavhan GB, Babyn PS, Thomas B, et al. Principles, techniques, and applications of T2*-based MR imaging and its special applications. *Radiographics*. 2009;29:1433–1449.
39. Wu LM, Chen XX, Xuan HQ, et al. Feasibility and preliminary experience of quantitative T2* mapping at 3.0 T for detection and assessment of aggressiveness of prostate cancer. *Acad Radiol*. 2014;21:1020–1026.
40. Miyata M, Aoki T, Shimajiri S, et al. Evaluation of the R2* value in invasive ductal carcinoma with respect to hypoxic-related prognostic factors using iterative decomposition of water and fat with echo asymmetry and least-squares emission (IDEAL). *Eur Radiol*. 2017;27:4316–4323.
41. Krishna MC, Subramanian S, Kuppusamy P, et al. Magnetic resonance imaging for in vivo assessment of tissue oxygen concentration. *Semin Radiat Oncol*. 2001;11:58–69.
42. Syed AK, Whisenant JG, Barnes SL, et al. Multiparametric analysis of longitudinal quantitative MRI data to identify distinct tumor habitats in preclinical models of breast cancer. *Cancer*. 2020;12.